Neurobiology of Disease 175 (2022) 105898

Contents lists available at ScienceDirect

Neurobiology of Disease

journal homepage: www.elsevier.com/locate/ynbdi

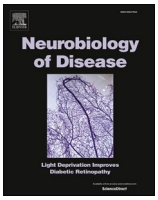

Reelin protects against pathological α-synuclein accumulation and dopaminergic neurodegeneration after environmental enrichment in Parkinson's disease

Eunju Cho [a,b,d,1], Kyungri Kim [a,d,1], Hyungtae Kim [a,c], Sung-Rae Cho [a,d,e,*]

[a] Department and Research Institute of Rehabilitation Medicine, Yonsei University College of Medicine, Seoul 03722, Republic of Korea
[b] Department of Psychological and Brain Sciences, Neuroscience and Behavior Program, University of Massachusetts Amherst, Amherst, MA, 01003, USA
[c] Department of Medicine, Yonsei University College of Medicine, Seoul 03722, Republic of Korea
[d] Brain Korea 21 PLUS Project for Medical Science, Yonsei University College of Medicine, Seoul 03722, Republic of Korea
[e] Graduate Program of Biomedical Engineering, Yonsei University College of Medicine, Seoul 03722, Republic of Korea

ARTICLE INFO

Keywords:
Parkinson's disease
α-synuclein
Environmental enrichment
Reelin
LAMP1

ABSTRACT

Two of the primary features of Parkinson's disease (PD) are the accumulation of α-synuclein (α-Syn) and the depletion of lysosomal-associated membrane protein 1 (LAMP1) in the brain. Beneficial effects of environmental enrichment (EE) have been reported on the activation of lysosomal function and the amelioration of PD symptoms. Furthermore, Reelin could be a novel therapeutic target in PD. Hence, in this study, we validated the effects of EE on the activation of LAMP1 *via* Reelin in PD. Heterogeneous α-Syn (A53T)-overexpressing transgenic mice (age 6 and 16 months) were exposed to EE for 8 weeks. After motor and cognitive tests, brain tissues were obtained from mice and subjected to immunohistochemistry and molecular analyses. EE ameliorated motor and non-motor symptoms, protected dopamine neurons, and reduced pathological α-Syn accumulation in the early stage of PD. Striatal Reelin levels were altered depending on the disease stage and regulated by EE in PD mice. To elucidate the underlying mechanism of the effect of EE on PD, we performed further molecular and cellular analyses using activated preformed fibril (PFF)-induced SH-SY5Y cells, an *in vitro* model of PD, which were treated with recombinant Reelin protein and a Reelin blocker, CR-50. The CR-50 increased pathological α-Syn accumulation and accelerated dopamine neuronal degeneration by decreasing LAMP1 in the PFF-induced PD model. Our results showed that Reelin increased LAMP1 after EE and decreased pathological α-Syn accumulation, thus protecting dopamine neurons from degeneration in the striatum and substantia nigra, and ameliorating neurobehavioral deficits. These results suggest that Reelin is a promising target in treating histopathological changes and improving behavioral symptoms associated with PD.

1. Introduction

Parkinson's disease (PD) is a progressive neurodegenerative disease accompanied by behavioral disturbances in motor and non-motor functions, including cognitive impairments (Cano-de-la-Cuerda et al., 2010; Goldman et al., 2018; Kim et al., 2017). It is commonly characterized by dopamine neuronal degeneration and phosphorylated α-synuclein (α-Syn^{pS129}) neuropathology in the striatum (STR) and substantia nigra pars compacta (SNpc) (Lotharius and Brundin, 2002; P. Damier et al., 1999; Venda et al., 2010; Xu and Pu, 2016). Although

Abbreviations: PD, Parkinson's disease; α-Syn, α-synuclein; LAMP1, lysosomal-associated membrane protein 1; EE, Environmental enrichment; PFF, preformed fibril; α-Syn^{pS129}, phosphorylated α-Syn; STR, striatum; SN, substantia nigra; SNpc, substatia nigra pars compacta; TH^{+}, tyrosine hydroxylase-positive; Tg, transgenic; DMEM, Dulbecco's modified Eagle's medium; FBS, fetal bovine serum; P/S, penicillin/streptomycin; PCR, polymerase chain reaction; PAT, passive avoidance task; NOR, Novel object recognition; RI, recognition index; qRT-PCR, Quantitative real-time PCR; IHC, immunohistochemistry; PBS, phosphate-buffered saline; BSA, bovine serum albumin; RT, room temperature; DAB, 3,3′-diaminobenzidine; DRD1, dopamine receptor D1; DRD2, dopamine receptor D2; Darpp32^{+}, dopamine- and cAMP-regulated neuronal phosphoprotein-positive..

* Corresponding author at: Department and Research Institute of Rehabilitation Medicine, Yonsei University College of Medicine, 50-1 Yonsei-ro, Seodaemun-gu, Seoul 03722, Korea.
E-mail addresses: eunjucho@umass.edu (E. Cho), kby930@yuhs.ac (K. Kim), kht20060@yuhs.ac (H. Kim), srcho918@yuhs.ac (S.-R. Cho).
[1] E.C. and K.K. equally contributed to this study.

https://doi.org/10.1016/j.nbd.2022.105898
Received 25 May 2022; Received in revised form 25 September 2022; Accepted 12 October 2022
Available online 18 October 2022

α-synuclein (α-Syn) has an essential role in homeostasis, many studies have confirmed that proteosomal dysfunction and lysosomal-associated membrane protein 1 (LAMP1)-associated endolysosomal pathway dysfunction lead to α-Syn aggregation and accumulation, resulting in increased toxic α-Syn^{pS129} aggregates and Lewy body neuropathology in the brain (Chu et al., 2009; Dehay et al., 2010; Dehay et al., 2013; Malik et al., 2019; Xilouri et al., 2016).

Basal ganglia perform as a center for motor control with dopaminergic signals from SNpc in healthy population. In PD, degeneration of dopaminergic neurons in SNpc instigates reduction in dopaminergic signal. Dopamine dysfunction in the basal ganglia is known to not only hinder motor function, but also affect non-motor symptoms in PD (McGregor and Nelson, 2019). Consequently, basal ganglia are a crucial control center to investigate the effects on motor and non-motor symptoms in PD (Middleton and Strick, 2000).

Progression of PD is determined by clinical manifestations and the extent of α-Syn inclusion (Braak et al., 2003; Parnetti et al., 2019; Poewe et al., 2017). Clinical stage of PD is subdivided into prodromal, early, mid, and late stage. Prodromal stage is characterized by non-motor symptoms including depression, anxiety, hyposmia, and constipation. As PD progresses into early stage, patients often experience motor impairments such as tremor, bradykinesia, and rigidity. Mid-stage symptoms involve dyskinesia, axial symptoms, and orthostatic hypotension. In the late stage, motor function is largely damaged. Patients experience worsening symptoms of dysphagia, postural instability, gait disturbance, and dementia (Poewe et al., 2017).

Clinical stage of PD is related to the progression of α-Syn inclusion, called Braak stage. Braak stage I and II involve accumulation of α-Syn in the lower brain stem. Braak stage III and IV result in presentation of motor symptoms due to α-Syn inclusion in midbrain and basal forebrain. As PD progresses into Braak stage V and VI, α-Syn inclusion accumulates in the limbic system and neocortex (Braak et al., 2003). Furthermore, it has revealed that the progression of PD changes in accordance to the oligomeric and phosphorylated α-Syn as potential cerebrospinal fluid (CSF) and blood biomarkers (Braak et al., 2003; Majbour et al., 2016; Parnetti et al., 2019; Poewe et al., 2017).

Environmental enrichment (EE) not only improves motor performance by providing physical exercise but also ameliorates non-motor symptoms by providing a variety of objects: sensory, cognitive, and social stimuli in the animal models of neurodegenerative diseases (Anastasía et al., 2009; Cechetti et al., 2012; De Giorgio, 2017; Gelfo et al., 2011; Huang et al., 2019; Livingston-Thomas et al., 2016; Marcon et al., 2018; Niethammer et al., 2013; Nygren and Wieloch, 2005; Rosenzweig et al., 1978; Tomlinson et al., 2013; Turner and Lewis, 2003; Wassouf and Schulze-Hentrich, 2019). EE imitates the stimuli of the treatment courses in the clinic provided to the patients by encouraging voluntary exercise, giving cognitive stimulation, and increasing social interaction (Janssen et al., 2014; Radabaugh et al., 2017; Sampedro-Piquero and Begega, 2017). Therefore, EE is used as an effective intervention for neurorehabilitation as a non-pharmacological therapy in traumatic brain injury, stroke, and drug addiction in patients and mouse models (Hamm et al., 1996; Pang et al., 2019; Peck et al., 2015; Qin et al., 2021).

Previous studies have shown that EE not only improved motor, cognitive, olfactory function, and synaptic plasticity but also reduced oxidative stress in a mouse model of PD (Kim et al., 2021; Seo et al., 2020; Wi et al., 2018). In addition, EE activated lysosomal function and protected neurons against degeneration and α-Syn disturbance in neurodegenerative diseases including PD (Anastasía et al., 2009; Huang et al., 2019). Furthermore, physical exercise could increase the Reelin expression and ameliorate motor deficits *via* Reelin-mediated anti-apoptotic effect (Kim et al., 2013). Reelin upregulation by EE activated its downstream molecules such as PI3K, p-ERK, and p-Akt, ultimately leading to an improvement in cognitive function (Seo et al., 2013).

Reelin is an extracellularly occurring glycoprotein that binds to the apolipoprotein E receptor 2 or very low-density lipoprotein receptors in the brain (Dlugosz and Nimpf, 2018; Rice and Curran, 2001). Activated Reelin signaling pathway enhances the migration, positioning, and growth of dendrite spines of neurons, including tyrosine hydroxylase-positive (TH^+) dopamine neurons in the brain (Arioka et al., 2018; Niu et al., 2008; Rice and Curran, 2001; Rogers et al., 2011; Sharaf et al., 2015). Reelin also promotes the release of neurotransmitters, including dopamine, through vesicle-associated membrane protein 7 protein activation, resulting in the regulation of synaptic strength in the presynapse compartment (Bal et al., 2013). Previous studies have reported that Reelin levels were altered in patients with Alzheimer's disease (AD) and PD compared to controls (Botella-López et al., 2006; Cho et al., 2021; Jesse et al., 2009; Lidón et al., 2020; Sáez-Valero et al., 2003). Moreover, Reelin was observed to attenuate insoluble amyloid β-protein aggregation and hyperphosphorylation of Tau protein accumulation in the brain of an AD animal model, resulting in cognitive functional improvement (Cuchillo-Ibañez et al., 2016; Pujadas et al., 2014).

Hence, this study assessed the effects of EE on attenuating α-Syn aggregation, protecting dopamine neurons against degeneration, and improving behavioral functions in the early stage of PD. To better understand the mechanism of the effect of EE on PD, we used an α-Syn (A53T)-overexpressing transgenic (Tg) mouse model in two different stages of the disease: early stage PD (age 6 months) and late stage PD (age 16 months). Further, we used *in vivo* and *in vitro* models to elucidate the role of Reelin as a novel therapeutic target in PD.

2. Materials and methods

2.1. Cell culture

SH-SY5Y (human neuroblastoma) cells were maintained in Dulbecco's modified Eagle's medium (DMEM)/F12 medium supplemented with 10% fetal bovine serum (FBS) and 1% penicillin/streptomycin (P/S; maintenance medium) in a humidified incubator at 37 °C with 5% CO_2. The culture medium was replaced every 2–3 days. When the cells reached 90% confluence, they were transferred to 48-well culture plates or to poly-D-lysine (0.1 mg/mL, Sigma)-coated coverslips and incubated overnight. The next day, SH-SY5Y cells were differentiated with retinoid acid (10 μM) in high-glucose DMEM (with 10% FBS and 1% P/S) for 4 days. For experiments involving Reelin treatment, differentiated SH-SY5Y cells were incubated with a culture medium containing preformed fibril (PFF) (5 μg/mL, StressMarq Biosciences), recombinant human Reelin protein (S1221-Q1226, R&D Systems, 8546-MR), and either normal rabbit IgG (4 μg/mL, Abcam, #2729) or CR-50 (4 μg/mL, MBL, D223–3) at different concentrations for 4 days (Gao et al., 2019; Volpicelli-Daley et al., 2011).

2.2. Cytotoxicity assay

For experiments involving cytotoxicity measurements, SH-SY5Y cells were seeded into 48-well culture plates and cell viability was evaluated with an ADAM-MC automated cell counter (Digital Bio Co., Ltd., NanoEnTek Inc.), according to the manufacturer's instructions. The numbers of total or non-viable cells were automatically calculated by the ADAM-MC software.

2.3. Animals

M83 Tg line mice (C57BL/6; *Prnp*-SNCA*A53T) overexpressing human A53T α-Syn *via* the mouse prion protein promoter were purchased from The Jackson Laboratory and maintained on a C57BL/C3H background. All animals were housed and provided water and food on a 12-h light/dark cycle according to animal protection regulations. In this study, both 4- and 14-month-old heterogeneous mice (female and male) were used, and behavioral tests were performed at age 6 and 16 months, respectively. No sex differences were observed in behavioral functions (**Supplementary Fig. S1** and **Additional file 2: Supplementary**

Fig. S2). All animal experiments were approved by the Institutional Animal Care and Use Committee of Yonsei University College of Medicine (approval no. 2018–0039, 2020–0026). The genotype of SNCA*A53T Tg mice was confirmed using real-time polymerase chain reaction (PCR) analysis. The SNCA*A53T transgene was amplified and detected using primer sequences provided by The Jackson Laboratory genotyping protocols database (protocol 18,858) (Giasson et al., 2002).

2.4. Environmental enrichment

EE contains a variety of novel objects that enhances physical, sensory, cognitive, and social stimuli in a large breeding cage (43 × 76 × 31 cm^3) than the standard cage (27 × 22.5 × 14 cm^3). The number of mice being bred in the EE cage was greater (5 to 7 mice per cage) than that of the standard laboratory cage (3 to 5 mice per cage) to create a social stimulus effect (Nithianantharajah and Hannan, 2006; Sampedro-Piquero and Begega, 2017).

EE cage includes running wheels to induce physical stimulus and toys of various colors and textures to induce sensory stimulus. Mice were exposed to a new environment, with their location of same objects changed at a weekly interval (Cechetti et al., 2012). According to a previous study, 4 weeks of EE exposure was sufficient to induce positive effects on cognition; however, old rodents required a longer exposure period (Sampedro-Piquero and Begega, 2017). Thus, 8 weeks of EE exposure was deemed appropriate as the experimental therapeutic approach in this study. Mice were randomly divided into the EE group and the standard housing group for 8 weeks. Female and male mice were housed separately.

2.5. Behavioral assessments

2.5.1. Rotarod test

Before the animals were exposed to EE, each mouse was placed on the rotarod apparatus (Ugo Basile, Italy) at a constant speed (10 rpm) for 20 min at age 4 or 14 months. After 8 weeks, mice were tested for locomotor activity at an accelerated speed (4–40 rpm) for 5 min. Three consecutive trials were performed, and the latency time to fall was recorded (Kim et al., 2013; Paumier et al., 2013). The mice were allowed to rest for 5 min between each trial.

2.5.2. Hanging wire grip test

Muscle strength was measured through a hanging wire test (Wang et al., 2020). Mice were placed on a thick metallic wire secured to two vertical stands. To avoid any vibration, the wire was firmly attached to the plastic frame. The wire was secured 35 cm above the wood shaving cage to prevent falling injury. The latency time to fall from the wire within 180 s was recorded, and each mouse was provided three trials with a 5-min rest between trials.

2.5.3. Ladder walking test

To assess the coordination/balance function of the forelimb and hind limb, a horizontal ladder (60 cm) with irregularly spaced metal rungs (Jeung Do B&P, Korea) was used. Mice were required to walk across the ladder three to four consecutive times. All trials were video recorded and analyzed by manually counting the number of reciprocal walking steps (Neureither et al., 2017; Xu, 2012).

2.5.4. Buried food test

Mice were deprived of food pellets for 18–24 h before the buried food test, in which the amount of time needed by the animals to find a food pellet hidden underneath a layer of bedding was measured (Wi et al., 2018; Yang and Crawley, 2009). Before performing the test, each mouse was individually placed in a clean holding cage for 5 min, transferred to the test cage for 2 min, and returned to the holding cage while a small pellet piece was hidden approximately 0.5 cm below the bedding at a random location. The animals were given 3 min to find the pellet, and the time it took the mice to start eating the food pellet was recorded.

2.5.5. Passive avoidance task (PAT)

A Plexiglas shuttle box (41.5 × 21 × 35 cm^3), as the PAT apparatus (Jeung Do B&P), was divided into bright and dark compartments separated by a guillotine door. The floor rods in the dark compartment were connected to an electrical stimulator. Mice were allowed 5 min to habituate to the environment of the apparatus during 2 consecutive days before inescapable shocks were delivered. For training, mice were allowed to explore the bright compartment for 30 s, at which point the guillotine door was raised to allow the mice to enter the dark compartment. An electrical shock (0.5 mA) was delivered for 2 s upon entry of the mouse to the dark compartment. Test sessions were performed to assess long-term memory (24 h later) at the age of 6 and 16 months, by recording the latency time to enter the dark compartment within 300 s.

2.5.6. Y-maze test

An enclosed Y-shaped maze (Jeung Do B&P) was used to evaluate spatial learning and memory (Deacon and Rawlins, 2006; Kraeuter et al., 2019; Magen et al., 2012; Paumier et al., 2013). Testing occurred in the opaque plastic arms at a 120-degree angle from each other, whereby wild-type mice generally would tend to investigate a new arm of the maze instead of returning to the previously explored one (Kraeuter et al., 2019). Same protocol to test for spontaneous alternation behavior was used to quantify cognitive deficits and recognition memory function for all mice groups. Each mouse was allowed to freely explore the maze for 8 min and monitored for the sequence of entries and the number of arm entries. An entry occurs when all 4 paws of the mouse have crossed over the half vertical length of the Y-maze arm (Tian et al., 2010). Percent of alteration was scored as follows: [Number of spontaneous alternation / (Number of total arm entries – 2)] × 100.

2.5.7. Novel object recognition (NOR) task

The NOR task involved the following three steps: habituation, familiarization, and test periods. For the habituation period, mouse activity monitoring was conducted in an empty white square box (30 × 30.5 × 31 cm^3) for 25 min (Leger et al., 2013; Lueptow, 2017; Magen et al., 2012). The next day, for familiarization, similar objects (a + a) were placed in the same side of the box and each mouse was allowed to freely explore the white box for 5 min. On the test day 24 h later, one of the familiar objects was replaced with a novel object of different shape and colour (a + a → a + b) at the same spot within the cage parameter. During the test period, automatic video recording was used to analyze sniffing behaviors and the exploration time spent on each object within 5 min. To assess learning and memory, the recognition index (RI) and the number of explorations of each object were analyzed. The discrimination rate was calculated as follows: RI = (time spent exploring a novel object [TN]–time spent exploring a familiar object [TF])/(TN + TF)), Number of entries to object zone = (number of explorations of a novel object [EN])/(number of explorations of both novel [EN] and familiar [EF] objects). Object zone means as follows: directing the nose toward the object at a distance less than or equal to 2 cm or touching the center of object with its nose.

2.6. Quantitative real-time PCR (qRT-PCR)

To evaluate the expression levels of target genes in the various brain regions, including the cortex and STR, total RNA was extracted using TRIzol (Invitrogen Life Technology, Carlsbad, CA, USA). After DNase digestion and clean-up, the RNA samples were evaluated for purity and the A260/A280 ratio was quantified using an Agilent 2100 Bioanalyzer (Agilent Technologies, Palo Alto, CA, USA). The extracted RNA samples were used to synthesize complementary DNAs (cDNAs) with ReverTra Ace® Qpcr RT Master Mix with gDNA Remover (TOYOBO, Osaka, Japan) using the following primers: mouse Reelin gene (*Reln*), forward

5′-CTGGTCCCTACTCCACACTG-3′ and reverse 5′-GCCAGAAAATCCTGGGTCAC-3′; mouse *gapdh*, forward 5′-TCACCACCATGGAGAAGGC-3′ and reverse 5′-GCTAAGCAGTTGGTGGTGCA-3′ (Moon et al., 2015). Thereafter, 1 μL cDNA was added in a total volume of 20 μL, as described in the LightCycler 480 (Roche Applied Science, Mannheim, Germany) datasheet. All experiments were performed in triplicate, and the gene expression level was calculated using the $2^{(-\Delta\Delta Ct)}$ method.

2.7. Tissue preparation and immunohistochemistry (IHC) staining

Animals were anesthetized with ketamine cocktail (100 mg/kg ketamine with 10 mg/kg Rompun, intraperitoneal injection) before obtaining brain tissue through transcardial perfusion. Transcardial perfusion was performed either with phosphate-buffered saline (PBS) infusion for molecular experiments or with PBS followed by 4% paraformaldehyde infusion for IHC analysis. First, mouse was anesthetized and its chest chamber opened. A 26-gauge needle with 25 mL syringe was injected into the left ventricle of mouse, with its right atrium punctured. Peripheral blood was removed with 50 mL of PBS infusion. Brain tissues were harvested in 30% sucrose at 4 °C until they sank. The brain tissues were cryosectioned at 25 μm thickness (Leica Biosystems Cryostat) and stained for IHC analysis as previously described (Nam et al., 2015). Briefly, the brain sections were washed with PBS three times for 10 min and rinsed with permeabilization solution (0.5% Triton X-100 [Sigma] and 0.5% bovine serum albumin [BSA; BOVOGEN] in PBS) two times at room temperature (RT) for 30 min. Thereafter, the sections were incubated with the primary antibody in blocking solution (1% BSA in PBS) at 4 °C overnight. The next day, the tissues were washed with PBS three times at RT for 10 min and incubated with biotin-conjugated IgG (H + L) secondary antibody (Vector Labs) in blocking solution at RT for 1 h. After the washing steps with PBS, three times at RT for 30 min, the tissues were incubated in avidin–biotin complex solution (Vector Labs) at RT for 1 h. The sections were rinsed with PBS three times. 3,3′-diaminobenzidine (DAB, Sigma) in 0.1 M phosphate buffer was used for signal detection after adding 0.003% H_2O_2 into the solution. DAB-stained tissues were washed with 0.1 M phosphate buffer, mounted on gelatin-coated microscope slides, dehydrated, coverslipped with Permount mounting medium (Fisher Chemical), and viewed under a bright-field microscope. For fluorescence microscopic analysis, fluorescence-conjugated secondary antibody was used to stain the tissues at RT for 1 h. After washing with PBS two times at RT for 15 min, the sections were mounted in anti-fade mounting medium with 4′,6-diamidino-2-phenylindole (VECTASHIELD, Vector Labs). Images obtained from a confocal microscope (Carl Zeiss) were analyzed using Image J software.

2.8. Thioflavin-S staining

To demonstrate the presence of aggregates, thioflavin-S staining was performed as previously described (Meadowcroft et al., 2015; Smith et al., 2014). For *in vitro* assay, SH-SY5Y cells seeded on poly-D-lysine-coated coverslips were washed with PBS, fixed with 4% paraformaldehyde for 30 min at RT, washed with filtered water (0.45 μm pore size, ADVANTEC) two times, and incubated with 0.05% thioflavin-S (Sigma) for 8 min at RT. The cells were rinsed with 80% ethanol three times and coverslipped with aqueous mounting medium (ScyTek Inc.). For *in vivo* assay, mouse brain sections were mounted onto gelatin-coated microscope slides, air dried, and washed with filtered water two times for 3 min. The brain tissue sections were incubated in filtered 1% aqueous thioflavin-S for 8 min at RT. The brain sections were rinsed with 80% ethanol two times for 3 min, 95% ethanol for 3 min, ion-exchanged distilled water three times, and coverslipped with aqueous mounting medium.

2.9. Immunoblot analysis

For immunoblot analysis, mouse STR tissues were homogenized and prepared as previously described (Yun et al., 2018). Briefly, non-ionic detergent-soluble proteins were prepared by homogenization with lysis buffer constituted by 10 mM Tris-HCl (pH 7.4), 150 mM NaCl, 5 mM EDTA, 0.5% NP-40, protease inhibitor cocktail (Cell Signaling Technology), and phosphatase inhibitor cocktail (GenDEPOT). The homogenized samples were centrifuged at 18,407 *g* for 15 min. The supernatant (soluble) was collected, and the pellet was washed, homogenized again with 1% sodium dodecyl sulfate- and 0.5% sodium deoxycholate-containing lysis buffer, and centrifuged at 30,100 *g* for 15 min. The supernatant (insoluble) was collected. For immunoblot analysis, immunoblots were prepared as previously described (Nam et al., 2015). Proteins in soluble fractions were used to evaluate the amount of Reelin protein through immunoprecipitation. Soluble brain fractions (500 mg) were incubated with the anti-Reelin primary antibody (Santa Cruz) for 4 h at 4 °C, followed by loading into protein G Sepharose™ fast flow column (GE Healthcare) overnight at 4 °C. Thereafter, the immunocomplexes were washed with lysis buffer, denatured by adding 2× lithium dodecyl sulfate sample buffer (Invitrogen), and boiled at 100 °C for <3 min.

2.10. Morphological analysis

The Multi Gauge software (version 3.0, Fujifilm) was used to measure the optical density of TH^+ striatal fibers (Nam et al., 2014). A fluorescence upright microscope (Olympus, BX43) was used for counting the total number of TH^+ neuronal cells in the SNpc region of the brain.

2.11. Statistical analysis

All data are expressed as mean ± standard error of the mean. Statistical analysis was performed with GraphPad Prism (version 8.4.2; GraphPad Software, La Jolla, CA, USA), and statistical significance was set at $p < 0.05$. All data were quantified relative to the α-Syn (A53T) Tg mouse group. IHC and immunoblot data were analyzed using one-way analysis of variance (ANOVA) followed by Tukey's multiple comparison test. The qRT-PCR results were analyzed using Student's *t*-test (unpaired). Behavioral data were analyzed using either one-way ANOVA followed by Tukey's multiple comparison test or Student's t-test to determine statistically significant differences.

3. Results

3.1. EE improved both motor and non-motor symptoms in the early stage but not cognitive symptoms in the late stage of PD in α-Syn (A53T) Tg mice

To test whether EE can improve motor and non-motor functions, we assessed olfactory function, grip hold strength, reciprocal ladder rung walking, and cognitive function in 6-month-old (early stage of PD) and 16-month-old (late stage of PD) α-Syn (A53T) Tg mice after 8 weeks of EE (Fig. 1A, B). EE remarkably decreased the latency to eat food in the buried food test, increased the latency to fall off a metal wire, and increased the number of reciprocal walking steps both in the early and late stages of PD in α-Syn (A53T) Tg mice (Fig. 1C–1H). In addition, EE significantly improved locomotor function in the accelerated rotarod test (Fig. 1N, P). Furthermore, to assess cognitive function, we conducted the Y-maze test, PAT, and NOR task. Importantly, EE significantly enhanced spatial learning and short-term memory, as shown from the increase in the spontaneous alternation ratio (Y-maze; Fig. 1B, I, K). EE also improved long-term memory, as shown from the prolonged retention time latency (PAT; Fig. 1J, L), and improved recognition memory, as shown from the increased time spent exploring and increased number of explorations of a novel object (NOR task; Fig. 1B) in

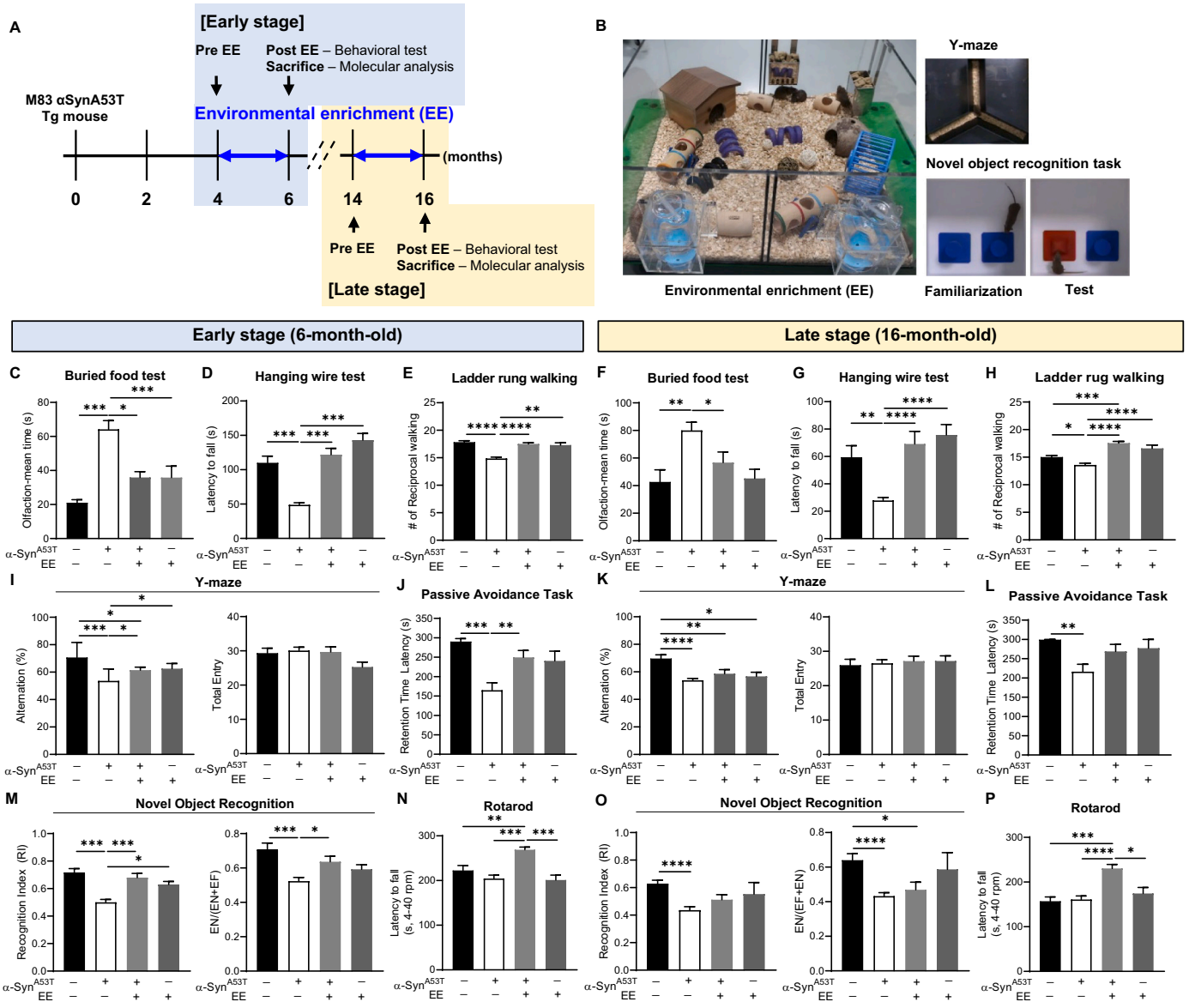

Fig. 1. EE enhanced motor and non-motor functions in early and late stage PD in α-Syn (A53T) Tg mice. Experimental scheme (A) and images (B) of the EE cage (left) and Y-maze and NOR test (right). Non-cognitive skill assessments for olfaction (C, F), grip strength (D, G), and reciprocal ladder rung walking test (E, H). Cognition behavioral tests: Y-maze (B, I, and K), PAT (J, L), and NOR (M, O). Measured latency time to fall off the rotarod in 6-month-old (N) and 16-month-old (P) mice. The maximum time was 300 s. 6-month-old mice, $n = 13$–44 per group;16-month-old mice, $n = 4$–37 per group. ****$p < 0.0001$ [C–E, J, M, N, P]; ***$p = 0.0004$ for F; ****p < 0.0001 for G and H; ****p < 0.0001 [alternation], $p = 0.0864$ [entry number] for I; ****p < 0.0001 [alternation], $p = 0.9469$ [entry number] for K; **$p = 0.0079$ for L; ***$p = 0.0002$ [RI] ***$p = 0.0001$ [EN] for O; Dataset is represented mean ± standard error of the mean (SEM). ****p < 0.0001, ***$p <$ 0.001, **$p < 0.01$, *$p < 0.05$, one-way ANOVA (Tukey's multiple comparison test). The detailed information about statistical analysis between groups and animal numbers are provided on Supplementary materials (Supplementary Table S1).

6-month-old (Fig. 1M) but not in 16-month-old α-Syn (A53T) Tg mice (Fig. 1O).

3.2. EE reduced monomeric α-Syn levels in the STR and phosphorylated serine 129 α-Syn levels in the SN of α-Syn (A53T) Tg mice in the early stage of PD

To confirm whether EE protects dopamine neurons and reduces pathological α-Syn expression levels depending on the PD stage, we analyzed TH^+ dopamine neurons, monomeric α-Syn levels, and $\alpha\text{-Syn}^{pS129}$ levels in the STR and SN through IHC and western blot analyses. In early stage of PD, EE protected TH^+ cell bodies by reducing monomeric and phosphorylated α-Syn accumulations in the SN (Figs. 2A–E **right**). Furthermore, EE prevented monomeric α-Syn accumulations in the STR (Fig. 2D **left**). TH^+ dopamine neuron cell fibers were intact and $\alpha\text{-Syn}^{pS129}$ was not detected by western blot analyses in the early stage of PD in the α-Syn (A53T) Tg mouse STR (Figs. 2A–C, 2E **left**). In the late stage of PD, EE ameliorated TH^+ dopamine neuronal degeneration and reduced monomeric and phosphorylated α-Syn in the SN (Figs. 2F–J **right**). However, EE did not significantly restore degenerated TH^+ cells and did not significantly decrease the $\alpha\text{-Syn}^{pS129}$ level in the STR (Figs. 2F–H, 2J **left**).

3.3. EE protected TH^+ dopamine neurons and reduced thioflavin-S^+ aggregated α-Syn in the early stage but not in the late stage of PD in the α-Syn (A53T) Tg mouse STR

Thioflavin-S staining demonstrated a similar change in protein

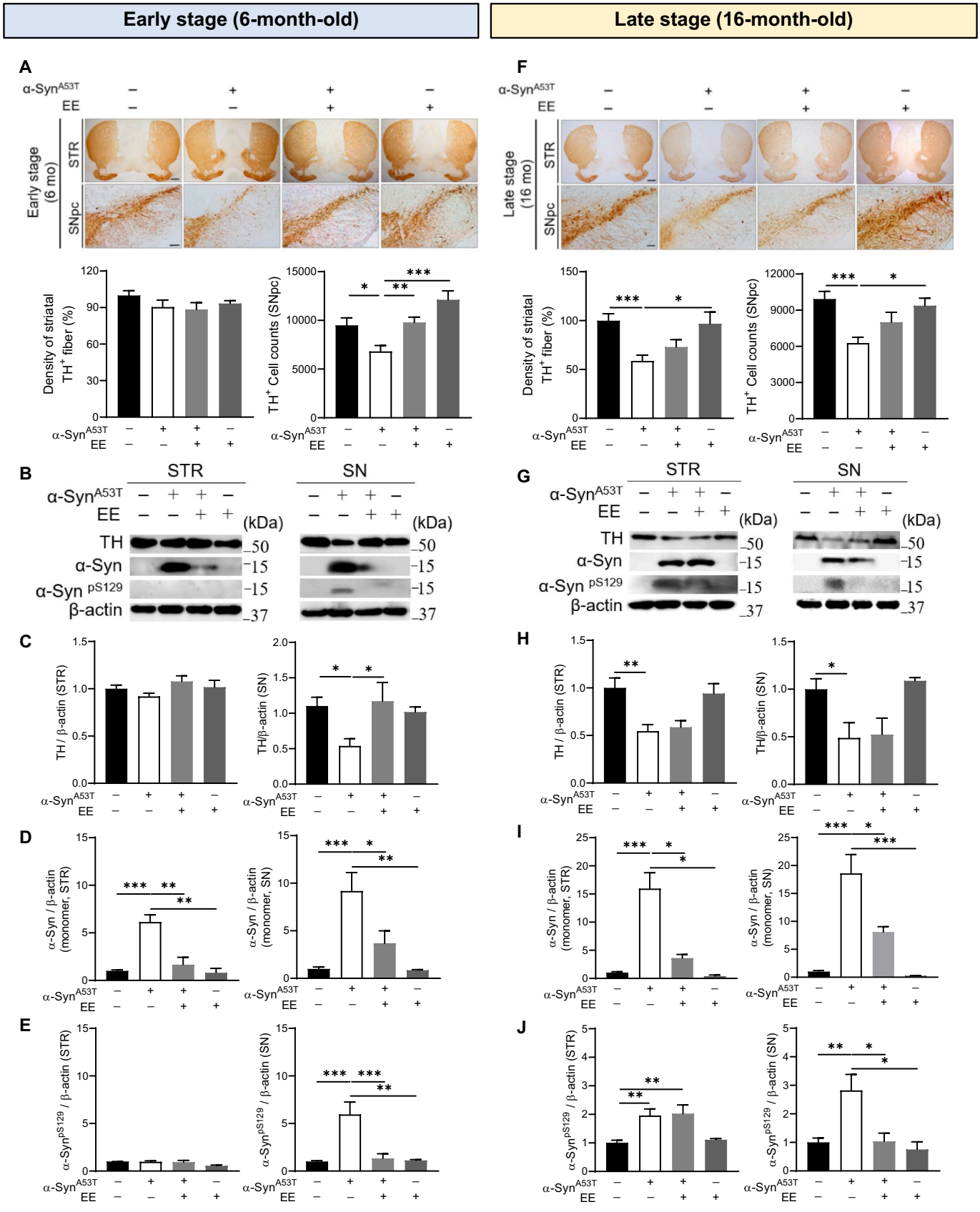

(caption on next page)

Fig. 2. EE protected TH$^+$ dopamine neurons and reduced α-Syn and phosphorylated α-Syn in the early stage of PD. (A, F) IHC images and analyses of TH+ dopamine neuron fibers (STR) and dopamine neuron cell bodies (SNpc) in the early (A) and late stages (F) of PD. [A], STR: $n = 5$–11 mice per group, $p = 0.9629$ and SNpc: n = 4–15 mice per group, ***$p = 0.0003$. [F], STR: n = 4–11 mice per group and SNpc: n = 4–13 mice per group, ***$p = 0.0006$. Scale bar, 500 μm (STR), 1 mm (SNpc). (B–E, G-J) Western blot images and analyses of TH, α-Syn, and α-SynpS129 in the mouse STR and SNpc in the early stage (B–E) and late stage (G–J) of PD. [B-E] $n = 3$–14 mice per group. $p = 0.0746$ *$p = 0.0268$ [C, STR and SN], ****$p < 0.0001$. For D and I *$p = 0.043$ ****p < 0.0001 [E, STR and SN], **$p = 0.0022$ *$p = 0.0174$ [H, STR and SN]. ****p = 0.0004 **$p = 0.0021$ [J, STR and SN]. Dataset is represented mean ± SEM. ****p < 0.0001, ***p < 0.001, **p < 0.01, *p < 0.05, one-way ANOVA (Tukey's multiple comparison test). The detailed information about statistical analysis between groups and animal numbers are provided on Supplementary materials (Supplementary Table S2). (For interpretation of the references to colour in this figure legend, the reader is referred to the web version of this article.)

aggregates in the STR and SNpc through EE. Importantly, the increased levels of thioflavin-S-stained aggregated proteins were significantly reduced after EE in the early stage of PD in the α-Syn (A53T) Tg mouse STR (Fig. 3A). However, in the late stage of PD, EE did not significantly reverse the level of aggregated proteins in the STR and SNpc (Fig. 3E). Immunofluorescence analyses were conducted to confirm that thioflavin-S$^+$ aggregated proteins were co-labeled with α-Syn or α-Syn^{pS129} in the STR and SNpc (Fig. 3B, F).

3.4. EE normalized dopamine receptors and LAMP1 levels in the early stage but not in the late stage of PD in the α-Syn (A53T) Tg mouse STR

Immunoblot analysis indicated that EE restored the disrupted levels of dopamine receptor D1 and D2 (DRD1, DRD2) expression to normal levels both in the early and late stages of PD in the α-Syn (A53T) Tg mouse STR (Fig. 3C, G). Therefore, we propose that early-life EE exposure could protect nigrostriatal dopamine neurons by preventing aggregated protein formation and accumulation that contribute to PD progression. To evaluate whether EE exposure can modulate LAMP1 in the STR, we evaluated LAMP1 expression levels using western blot analysis (Fig. 3D, H). The results showed that EE significantly increased the striatal LAMP1 expression in the early stage of PD in α-Syn (A53T) Tg mice but not in the late stage, suggesting that EE regulates striatal Reelin and LAMP1$^+$ lysosome functions in the early stage of PD.

3.5. EE restored Reelin expression in the early stage of PD in the α-Syn (A53T) Tg mouse STR

To confirm whether Reelin expression changes depending on the disease stage, we analyzed the brain tissues of 6-month-old (early stage) and 16-month-old (late stage) α-Syn (A53T) Tg mice. The relative Reelin mRNA (*Reln*) and Reelin protein (180-kDa band) expression levels were assessed in various brain regions including the STR, cortex, and olfactory bulb (Fig. 4). In the early stage of PD (age 6 months), qRT-PCR showed significantly increased levels of *Reln* in the STR and in the olfactory bulb but not in the cortex of α-Syn (A53T) Tg mice (Fig. 4A–C). In contrast, in the late stage of PD (age 16 months), the *Reln* levels were significantly decreased in the STR, cortex, and olfactory bulb. We confirmed the protein levels of Reelin using western blot and immunofluorescence analyses. Similar to the *Reln* levels, the Reelin levels were increased in the early stage but decreased in the late stage of PD in the STR of α-Syn (A53T) Tg mice (Fig. 4D, G). These results suggest that the *Reln* and Reelin levels change depending on the PD stage in α-Syn (A53T) Tg mice. Moreover, to test whether EE ameliorates abnormal Reelin levels in the brain, the animals were exposed to EE for 8 weeks. We found that EE remarkably restored Reelin expression to the normal levels both in the early and late stages of PD in the STR of α-Syn (A53T) Tg mice (Fig. 4D, G). The IHC results, consistent with those of western blot analyses, showed that EE restored Reelin expression to the normal levels in dopamine- and cAMP-regulated neuronal phosphoprotein-positive (Darpp32$^+$) medium spiny neurons in the α-Syn (A53T) Tg mouse STR (Fig. 5). No changes were observed in the cortex and olfactory bulb (Fig. 4E–F, 4H–I).

3.6. Reelin decreased α-Syn accumulation and protected TH$^+$ dopamine neurons by increasing LAMP1 in PFF-treated SH-SY5Y cells

To determine the mechanistic association of Reelin and LAMP1 in reducing aggregated α-Syn accumulation, we designed an *in vitro* study using recombinant Reelin protein and Reelin-neutralizing antibody (CR-50) in PFF-treated SH-SY5Y cells as a model of PD (Fig. 6A) (Gao et al., 2019; Volpicelli-Daley et al., 2011). The CR-50 level was determined by measuring the levels of activated phosphorylated DAB1 (**Supplementary Fig. S3**) (Moon et al., 2015; Qiu et al., 2006). Immunocytochemistry analysis showed that Reelin inhibition by CR-50 significantly decreased LAMP1, resulting in accumulated α-Syn aggregation in PFF-treated SH-SY5Y cells (Fig. 6B, C). Similarly, western blot analysis showed that blocking the Reelin function did not induce LAMP1 expression, resulting in enhanced monomer and oligomer α-Syn accumulations (Fig. 6D, F–H). Furthermore, inhibition of Reelin function failed to protect TH$^+$ dopamine neurons in PFF-treated SH-SY5Y cells (Fig. 6D, E), indicating that Reelin prevents dopamine neuronal degeneration *via* LAMP1 by reducing abnormal α-Syn accumulation in a PFF-induced *in vitro* PD model.

4. Discussion

EE has emerged as a promising therapeutic approach for neurodegenerative diseases. Numerous studies have shown that EE improves brain function by enhancing motor and cognitive stimulation, promoting dopamine neuroprotection, and activating lysosome function, thus reducing the risk of PD or delaying its progression (Barak et al., 2013; Gelfo et al., 2011; Huang et al., 2019; Marcon et al., 2018; Sampedro-Piquero and Begega, 2017; Tsukita et al., 2021; Wassouf and Schulze-Hentrich, 2019). In the early stage of PD, olfactory impairment, muscle weakness, balance deterioration, cognitive dysfunction, and locomotor activities were improved by EE; however, cognitive deficits were not improved by EE in the late stage (Fig. 1). These results indicate that EE prevents both motor and non-motor deficits in the early stage, but it does not ameliorate cognitive deficits in the late stage of PD.

When foot fault scoring was conducted in the ladder rung walking test, there was no significant difference between WT and a-Syn (A53T) in standard cages. However, the number of faults decreased significantly when both WT and a-Syn (A53T) Tg mice groups were exposed to EE (**Supplementary Fig. S4**). Previous report similarly revealed that there has been no significant difference between PD and healthy animals in the slips or misses of ladder rungs steps (Bourdenx et al., 2015). However, reciprocal walking was used to conduct as a more sensitive gait analysis (Wenger et al., 2022). There exists a more specific scoring system to analyze ladder rung walking test, which can be evaluated in future studies (Martins et al., 2022; Metz and Whishaw, 2002).

As behavioral assessments were compared between WT and a-Syn (A53T) Tg mice groups, mice showed a greater deterioration in motor symptoms in the late stage as compared to the early stage. However, there were no significant difference in non-motor symptoms for all groups (**Supplementary Fig. S5**). Early stage of PD reflected intact TH$^+$ dopaminergic neuron fibers, increased α-Syn aggregates, absence of α-Syn^{pS129} protein in the STR, decreased TH$^+$ dopamine neuronal cell bodies, increased levels of α-Syn aggregates, and observation of α-Syn^{pS129} in the SN **(**Figs. 2A–E, and 3A–B**).** In the late stage of PD

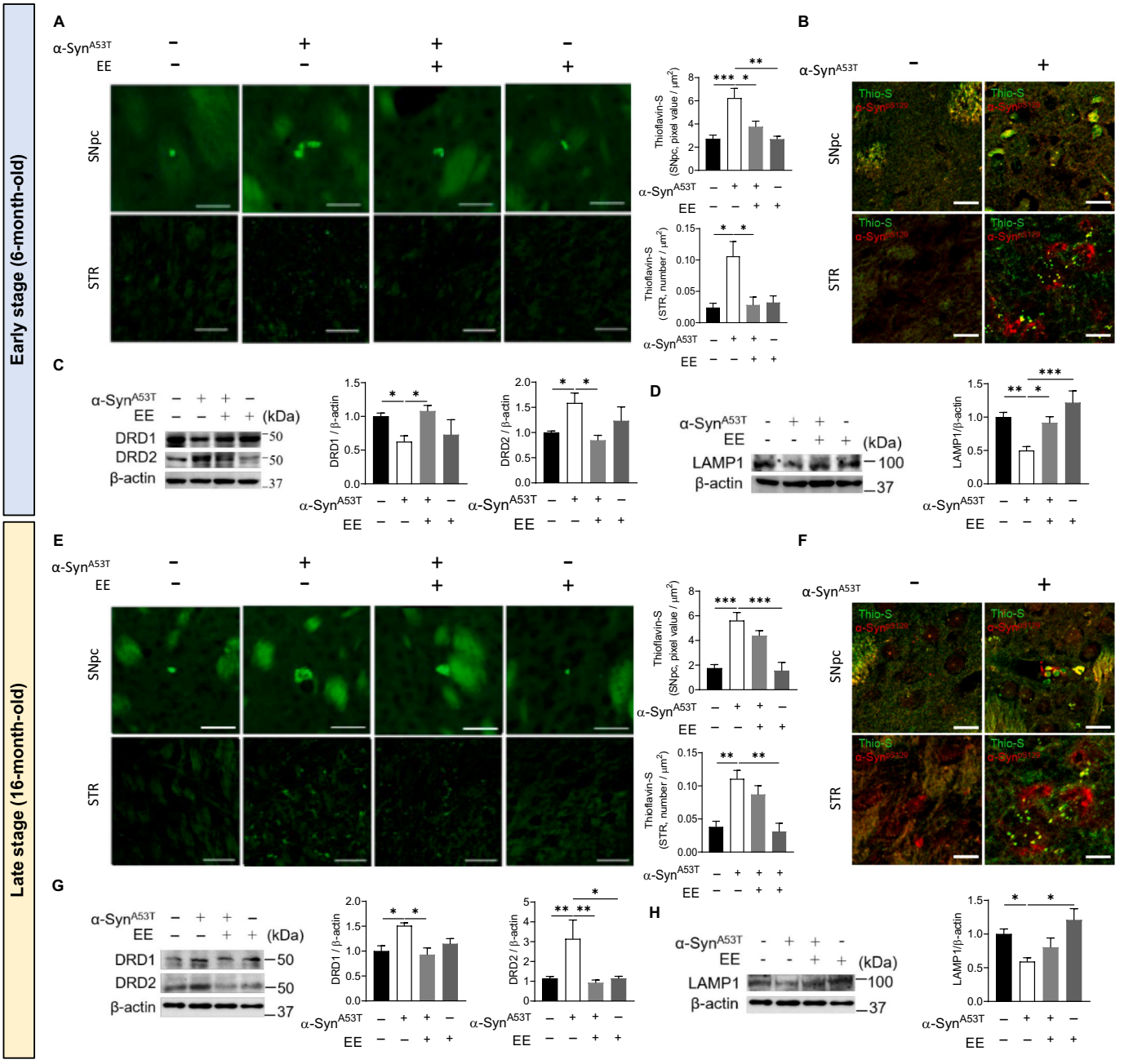

Fig. 3. EE decreased thioflavin-S^{+} α-Syn aggregations and normalized dopamine receptor and LAMP1 levels in STR in early but not late stage PD. (A, E) Thioflavin-S staining images and analyses of mouse STR and SNpc in the early stage (A) and late stage (E) of PD. [A] STR: n = 3–5 mice per group, $*p = 0.0132$; SNpc: n = 4–7 mice per group, $**p = 0.0042$. [E] STR: n = 4–11 mice per group, $**p = 0.0014$; SNpc: n = 4–7 mice per group, $***p = 0.0002$. Scale bar, 50 μm. (B, F) Immunofluorescence images of thioflavin-S and either α-Synnor (normal α-Syn) in the early stage of PD or α-SynpS129 (phosphorylated α-Syn [pS129]) in the late stage of PD in the mouse STR and SNpc. Scale bar, 15 μm. (C, G) Western blot images and analyses of DRD1 and DRD2 in the mouse STR in the early stage (C) and late stage (G) of PD. n = 3–8 mice per group. [C] $**p = 0.0054$ for DRD1, $*p = 0.0126$ for DRD2; [G] $*p = 0.0142$ for DRD1, $**p = 0.0052$ for DRD2. (D, H) Western blot images and analyses of LAMP1 in the mouse STR in the early stage (D) and late stage (H) of PD. [D], n = 3 or 6 mice per group, ***p = 0.0003; [H], n = 3–8 mice per group, $**p = 0.0098$. Dataset is represented mean ± SEM. ***p < 0.001, **p < 0.01, *p < 0.05, one-way ANOVA (Tukey's multiple comparison test). The detailed information about statistical analysis between groups and animal numbers are provided on Supplementary materials (Supplementary Table S3). (For interpretation of the references to colour in this figure legend, the reader is referred to the web version of this article.)

brain, not only degeneration of both TH^{+} dopaminergic neuron fiber density and cell bodies but also significantly increased levels of α-Syn aggregates, and α-Syn^{pS129} were observed in the STR and SN (Figs. 2F–J, and 3E–F). In α-Syn (A53T) Tg mice, TH^{+} dopaminergic fiber and cells were reduced in STR and SN in a greater value in the late stage as compared to the early stage. More α-Syn aggregates were discovered in STR (**Supplementary Fig. S6**). In the early stage of PD, exposure to EE has significantly decreased abnormal α-Syn accumulations and protected TH^{+} dopaminergic fiber and cells in the STR and SN in the early stage of PD. However, in the late stage of PD, EE failed to decrease α-Syn^{pS129} and α-Syn aggregates and to protect dopaminergic neurons against degeneration. Such results implicate that, in the early stage of PD, EE can protect TH^{+} dopamine neurons in the nigrostriatal pathway and may contribute to attenuating aggregated protein formation and

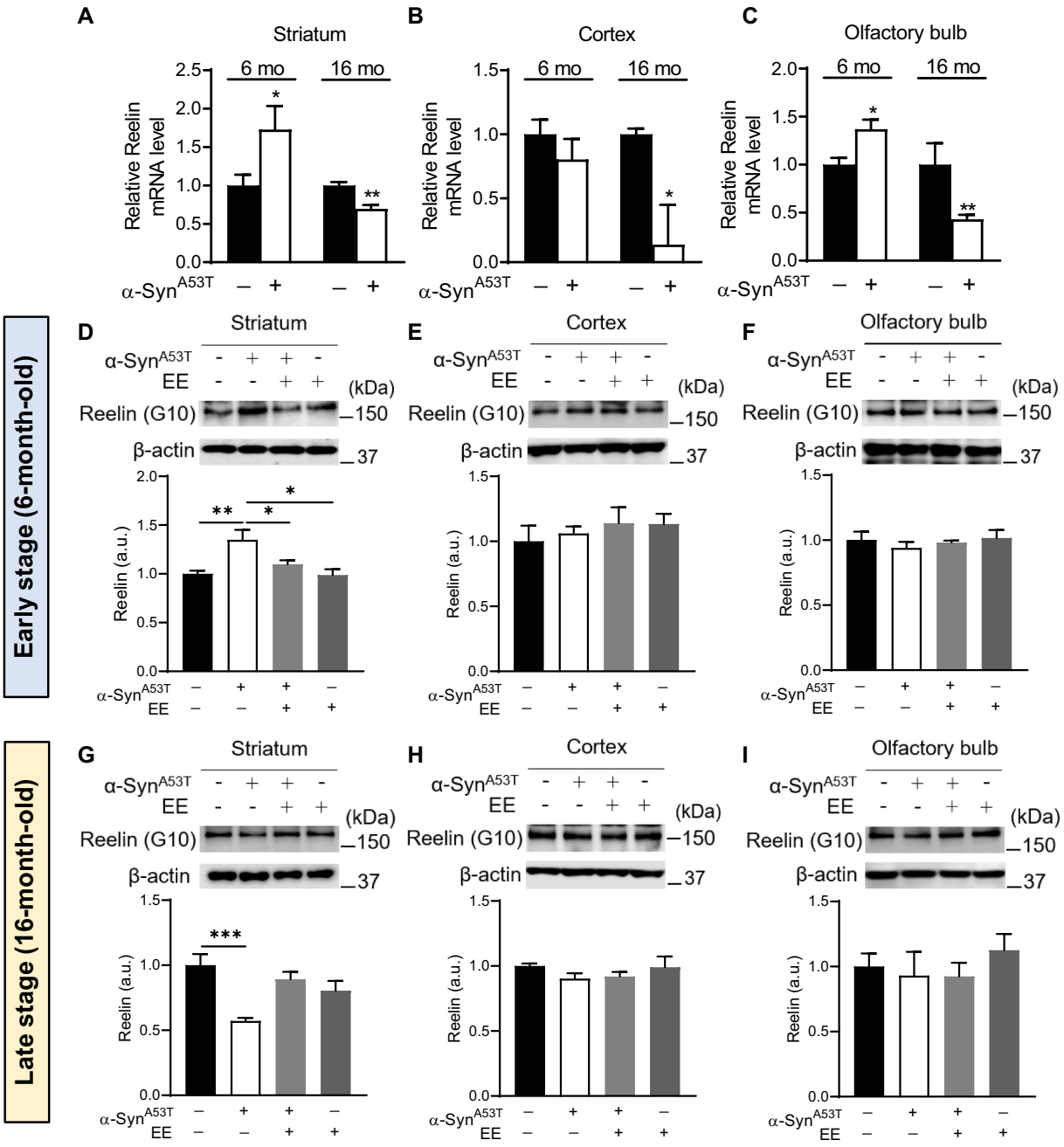

Fig. 4. EE normalized Reelin levels in early and late stage PD in α-Syn (A53T) Tg mouse STR (Western blot). (A–C) qRT-PCR analyses of relative *Reln* (Reelin mRNA) expression levels in the early and late stages of PD in the mouse striatum. n = 3–6 per group for 6-month-old mice, n = 3–5 per group for 16-month-old mice. [A], $*p = 0.0378$ for 6-month-old mice $**p = 0.0052$ for 16-month-old mice; [B], $*p = 0.034$ for 16-month-old mice; [C], $*p = 0.0434$ for 6-month-old mice $*p = 0.0476$ 16-month-old mice. Data are mean ± SEM. Student's *t*-test (unpaired). Western blot images (upper) and analyses (lower) of Reelin in the mouse brain in the early stage (D–E) and late stage (G–I) of PD. [D], n = 4–13 mice per group, $**p = 0.0012$; E, n = 3–6 mice per group, $p = 0.4941$; [F], n = 3 mice per group, $p = 0.7533$; [G], n = 3–8 mice per group, $***p = 0.0004$; [H and I], n = 3 mice per group, $p = 0.4635$). Dataset is represented mean ± SEM. $***p < 0.001$, $**p < 0.01$, $*p < 0.05$, one-way ANOVA (Tukey's multiple comparison test). The detailed information about statistical analysis between groups and animal numbers are provided on Supplementary materials (Supplementary Table S4).

accumulation in both the STR and SN.

Increasing evidences demonstrate that disrupted levels of DRD1, DRD2 are associated with symptoms of PD (Graham and Sidhu, 2010; Rassu et al., 2017; Unger et al., 2006). EE restored the dopamine receptors DRD1 and DRD2 to the normal protein levels in both stages of PD (Fig. 3C, G). This is in line with the previous results, whereby a decrease in both dopamine level and TH^+ optical density in the STR of PD mice were observed (Kilpeläinen et al., 2019). Therefore, the striatal dopamine neuronal fiber denervation presents a strong implication that the dopamine level may be profoundly reduced in the late stage of PD, leading to DRD augmentation in the STR (Calabresi et al., 2007; Ułas and Cotman, 1996). There has been no difference in α-Syn aggregates, DRD1, and DRD2 expressions in WT mice according to the periodical assessment. Conversely, the expressions showed a significant change in α-Syn (A53T) Tg mice over a period (**Supplementary Fig. S7**).

Previous studies have shown that TH^+ dopamine neurons express Reelin during mouse brain development (Arioka et al., 2018; Sharaf et al., 2015). Reelin level changes in the brain and CSF of patients with

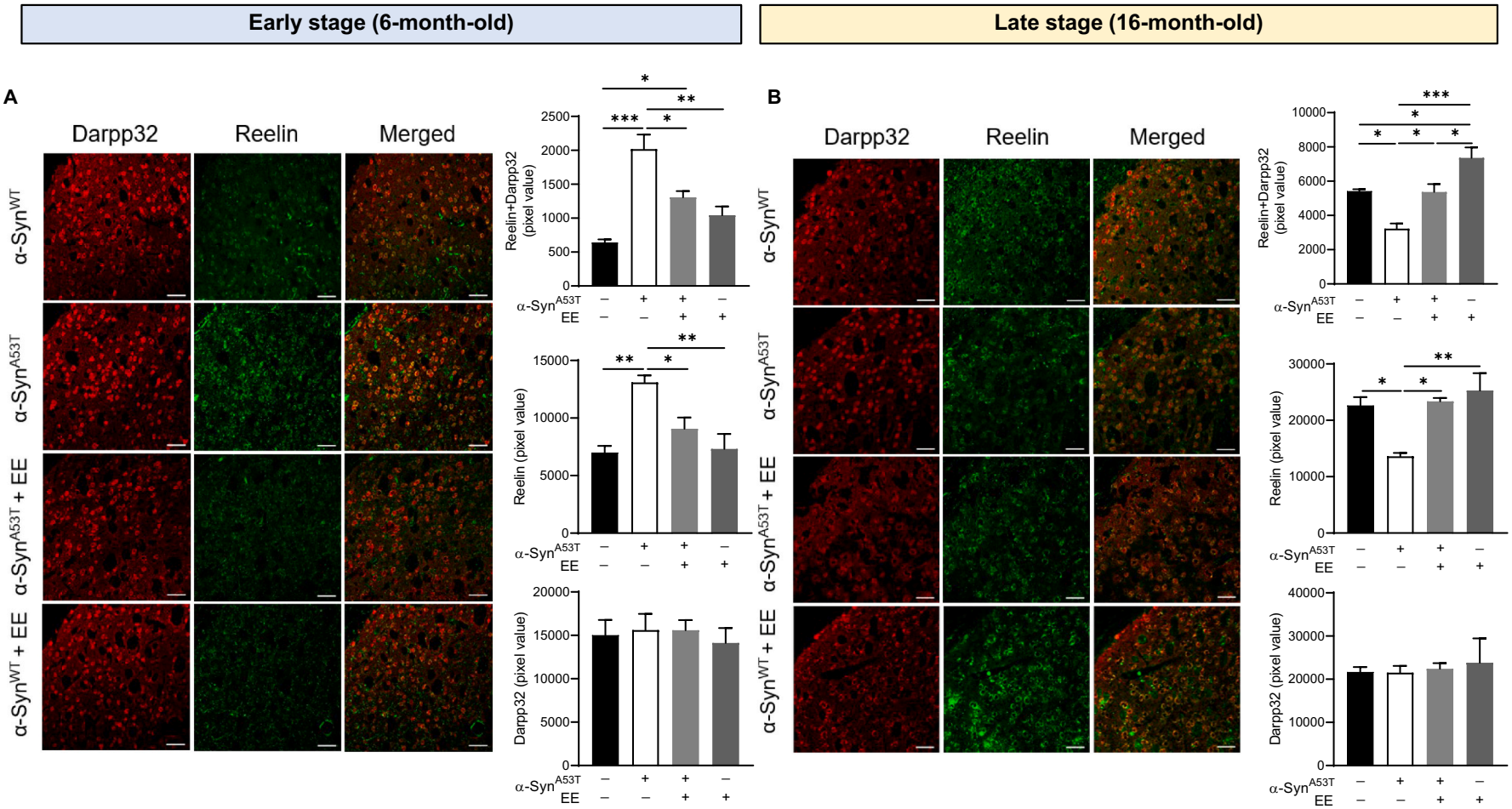

Fig. 5. EE normalized Reelin and Darpp32 expression in early and late stage PD in α-Syn (A53T) Tg mouse STR (Immunohistochemistry). Immunofluorescence images and quantifications of Reelin and Darpp32 in the α-Syn (A53T) Tg mouse STR in the early stage (A) and late stage (B) of PD. Scale bar, 50 μm. [A], n = 3 mice per group, ***p = 0.0004 for Reelin+/Darpp32+, **$p = 0.0015$ for Reelin, $p = 0.8808$ for Darpp32; [B], n = 3 or 4 mice per group, ***p = 0.0003 for Reelin+/Darpp32+, **p = 0.0054 for Reelin, $p = 0.8299$ for Darpp32. Dataset is represented mean ± SEM. ***p < 0.001, **p < 0.01, *p < 0.05, one-way ANOVA (Tukey's multiple comparison test). The detailed information about statistical analysis between groups and animal numbers are provided on Supplementary materials (Supplementary Table S5). (For interpretation of the references to colour in this figure legend, the reader is referred to the web version of this article.)

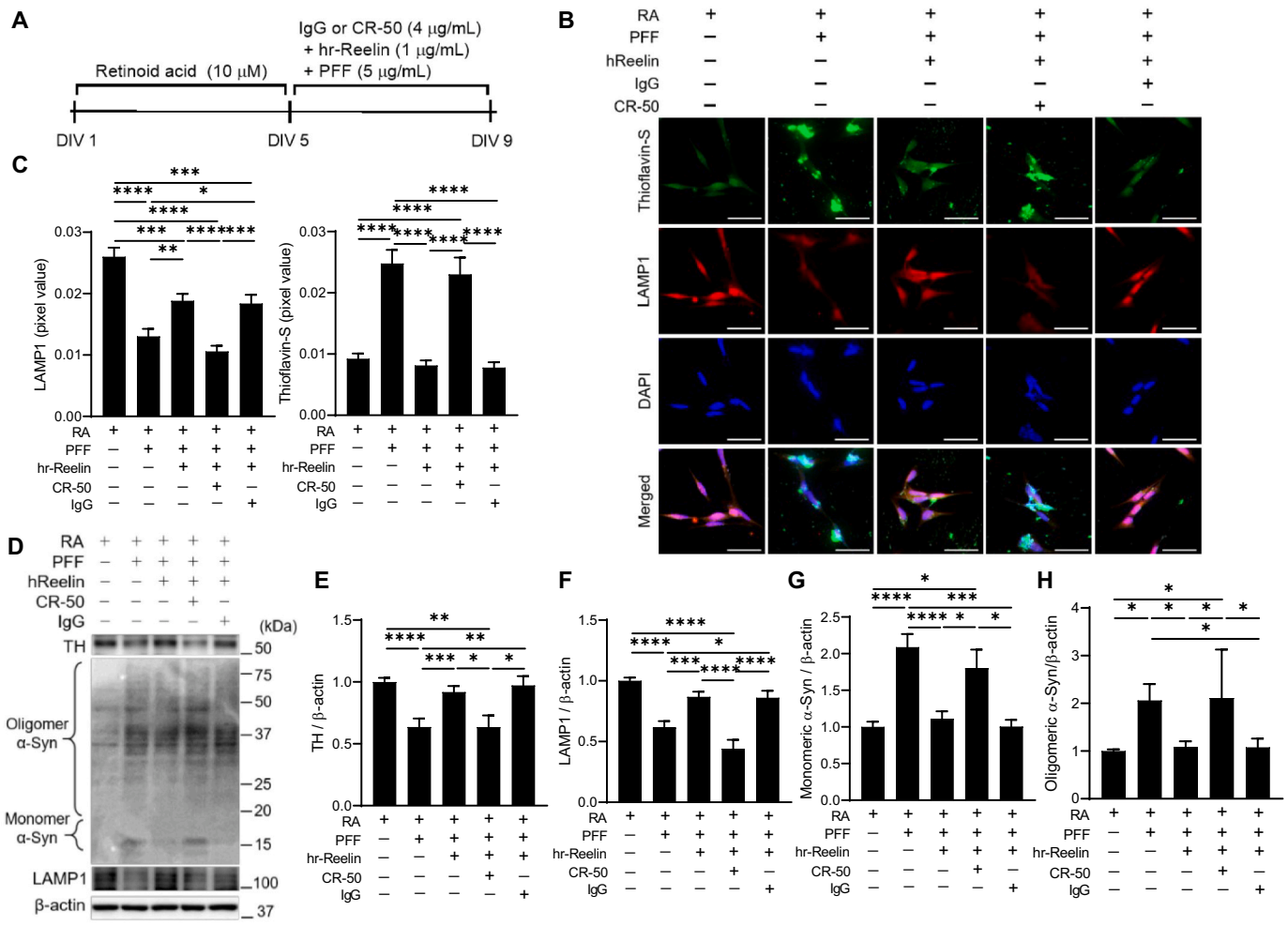

Fig. 6. Reelin-neutralizing antibody, CR-50, selectively depleted LAMP1 and accelerated α-Syn accumulation in PFF-treated SH-SY5Y cells. (A) Schematic diagram of the experimental design. Cells were incubated with hr-Reelin and IgG or hr-Reelin and CR-50 (4 μg/mL) for 2 h, followed by incubation in PFF (2 μg/mL) for 4 days. (B) Representative immunofluorescence images of aggregated α-Syn protein (thioflavin-S, green), LAMP1 (red), and 4′,6-diamidino-2-phenylindole (DAPI; blue) in SH-SY5Y cells. Scale bar, 50 μm. (C) The intensity of cells with thioflavin-S and LAMP1 were analyzed. $n = 40$–54 cells/group. (D—H) Representative images (D) and quantifications (E–H) of tyrosine hydroxylase (anti-TH), monomeric α-Syn (anti-α-Syn), oligomeric α-Syn (anti-Syn211), and LAMP1 (anti-LAMP1) protein levels in SH-SY5Y cells. $n = 6$–17 per group. [*E*-G] ****p < 0.0001. [H] ***$p = 0.0009$. Dataset is represented mean ± SEM. ****p < 0.0001, ***p < 0.001, **p < 0.01, *p < 0.05, one-way ANOVA (Tukey's multiple comparison test). The detailed information about statistical analysis between groups and animal numbers are provided on Supplementary materials (Supplementary Table S6). (For interpretation of the references to colour in this figure legend, the reader is referred to the web version of this article.) (For interpretation of the references to colour in this figure legend, the reader is referred to the web version of this article.)

neurodegenerative diseases such as AD and PD (Botella-López et al., 2006; Jesse et al., 2009). In addition, therapeutic effects of Reelin in an *in vitro* model of PD were shown by attenuating cell senescence and pathological α-Syn expression (Cho et al., 2021). This study provides evidence that EE regulates Reelin expression in the STR of PD (Figs. 4, 4D–I and 5). Specifically, there was no difference in Reelin in the STR of WT mice but Reelin was significantly reduced in the late stage of PD instead of the early stage (**Supplementary Fig. S8**). These results suggest that EE may be a promising therapeutic strategy for α-Syn-induced PD by normalizing striatal Reelin expression patterns in α-Syn (A53T) Tg mice.

We further elucidated a possible mechanism involving Reelin-mediated pathological α-Syn degradation *via* LAMP1 in the STR, resulting in the protection of dopaminergic neurons in both the STR and SN (Figs. 4 and 5). With LAMP1 upregulated by the recombinant Reelin protein, total α-Syn and aggregated α-Syn accumulations were reduced, and dopamine neurons were protected against degeneration in an *in vitro* model of PFF-induced PD (SH-SY5Y cells) (Figs. 6A–C). We also confirmed that the Reelin-neutralizing antibody CR-50 prevented LAMP1 upregulation, leading to increased pathological α-Syn accumulation and to decreased dopamine neurons (Figs. 6D–H). This *in vitro* study provided clear evidence that Reelin is involved in pathological α-Syn degradation and dopamine neuron protection by upregulating LAMP1. Therefore, this study provided further insights into the function of Reelin associated with the stage-dependent progression of PD.

Therapeutic effect of Reelin is confirmed in PFF-induced PD *in vitro* model and in early stage of α-Syn (A53T) Tg PD *in vivo* model by EE. However, in late stage of PD, the exposure of EE neither protected dopaminergic neurons nor decreased the level of phosphorylated α-Syn in the α-Syn (A53T) Tg mouse STR. This possibly could serve to clarify the assumption that, in early stage of disease, the increased requirement of Reelin induces the increased expressions of mRNA and protein to protect dopamine neurons, while in late stage of disease state it failed to further release of Reelin due to the degeneration of cells including dopaminergic neurons with aging. Therefore, it is important to apply EE at an early stage of PD as a treatment when dopamine neuronal fibers are remained. However, more *in vivo* studies are needed to evaluate the relevance of Reelin to behavioral function improvements using *Reln* knockout mice or *Reln* knockdown virus.

This study suggests that early-life exposure to EE would bring more

positive results in preventing the progression of behavioral symptoms and in protecting dopaminergic system functions than later-life EE exposure in PD. Moreover, the level of striatal Reelin, which is regulated by EE, can be used as an indicator for predicting the stage of PD progression and for deciding treatment and could be a novel therapeutic target to activate the pathological α-Syn degradation pathway in PD.

5. Conclusion

EE normalized striatal Reelin expression in the α-Syn (A53T) mouse model of PD, protecting dopamine neurons against degeneration in the early stage of PD. Particularly, EE not only decreased pathological α-Syn formation and increased LAMP1 in the brain but also improved behavioral functions. *In vitro* study confirmed that Reelin protected dopamine neurons and reduced α-Syn aggregation by increasing LAMP1. These results suggest that Reelin is a promising target in treating histopathological changes and improving behavioral symptoms associated with PD.

Ethics approval and consent to participate

All animals were housed in a facility accredited by the Association for Assessment and Accreditation of Laboratory Animal Care (AAALAC). Experimental procedures were approved by the Institutional Animal Care and Use Committee (IACUC 2018-0039, IACUC 2020-0026).

Consent for publication

Not applicable.

Availability of data and material

All relevant data that support the findings of this study are available from the corresponding author upon reasonable request.

Funding

This research was supported by the Korean Fund for Regenerative Medicine (KFRM) grant funded by the Ministry of Science and ICT, the Ministry of Health & Welfare, Republic of Korea [21A0202L1, 21C0715L1]; the Korean Health Technology R&D Project through the Korea Health Industry Development Institute (KHIDI), funded by the Ministry of Health & Welfare, Republic of Korea [HI21C1314]; and the faculty research grant of Yonsei University College of Medicine [6-2020-0104].

CRediT authorship contribution statement

Eunju Cho: Conceptualization, Investigation, Writing – original draft, Visualization. **Kyungri Kim:** Investigation, Formal analysis, Writing – review & editing. **Hyungtae Kim:** Investigation, Formal analysis. **Sung-Rae Cho:** Writing – original draft, Supervision, Project administration, Funding acquisition.

Declaration of Competing Interest

We declare that we do not have any commercial or associative interest that represents a conflict of interest in connection with the work submitted.

Data availability

The data that has been used is confidential.

Acknowledgments

We thank Editage (www.editage.co.kr) and Jihye Hwang for English language editing, Siwoo Lee for assisting with behavioral assessments.

Appendix A. Supplementary data

Supplementary data to this article can be found online at https://doi.org/10.1016/j.nbd.2022.105898.

References

Anastasía, A., et al., 2009. Enriched environment protects the nigrostriatal dopaminergic system and induces astroglial reaction in the 6-OHDA rat model of Parkinson's disease. J. Neurochem. 109, 755–765.
Arioka, Y., et al., 2018. Single-cell trajectory analysis of human homogenous neurons carrying a rare RELN variant. Transl. Psychiatry 8, 129.
Bal, M., et al., 2013. Reelin mobilizes a VAMP7-dependent synaptic vesicle pool and selectively augments spontaneous neurotransmission. Neuron. 80, 934–946.
Barak, B., et al., 2013. Opposing actions of environmental enrichment and Alzheimer's disease on the expression of hippocampal microRNAs in mouse models. Transl. Psychiatry 3, e304.
Botella-López, A., et al., 2006. Reelin expression and glycosylation patterns are altered in Alzheimer's disease. Proc. Natl. Acad. Sci. U. S. A. 103, 5573–5578.
Bourdenx, M., et al., 2015. Lack of additive role of ageing in nigrostriatal neurodegeneration triggered by α-synuclein overexpression. Acta Neuropathol. Commun. 3, 1–15.
Braak, H., et al., 2003. Staging of brain pathology related to sporadic Parkinson's disease. Neurobiol. Aging 24, 197–211.
Calabresi, P., et al., 2007. Dopamine-mediated regulation of corticostriatal synaptic plasticity. Trends Neurosci. 30, 211–219.
Cano-de-la-Cuerda, R., et al., 2010. Is there muscular weakness in Parkinson's disease? Am. J. Phys. Med. Rehabil. 89, 70–76.
Cechetti, F., et al., 2012. Environmental enrichment prevents behavioral deficits and oxidative stress caused by chronic cerebral hypoperfusion in the rat. Life Sci. 91, 29–36.
Cho, E., et al., 2021. Reelin alleviates mesenchymal stem cell senescence and reduces pathological α-Synuclein expression in an in vitro model of Parkinson's disease. Genes (Basel) 12, 1066.
Chu, Y., et al., 2009. Alterations in lysosomal and proteasomal markers in Parkinson's disease: relationship to alpha-synuclein inclusions. Neurobiol. Dis. 35, 385–398.
Cuchillo-Ibañez, I., et al., 2016. The β-amyloid peptide compromises Reelin signaling in Alzheimer's disease. Sci. Rep. 6, 31646.
Damier, P., Agid, E.C.H.Y., Gaybiel, A.M., 1999. The substantia nigra of the human brain II. Patterns of loss of dopmaine-containing neurons in Parkinson's disease. Brain 122, 1437–1448.
De Giorgio, A., 2017. The roles of motor activity and environmental enrichment in intellectual disability. Somatosens. Mot. Res. 34, 34–43.
Deacon, R.M., Rawlins, J.N., 2006. T-maze alternation in the rodent. Nat. Protoc. 1, 7–12.
Dehay, B., et al., 2010. Pathogenic lysosomal depletion in Parkinson's disease. J. Neurosci. 30, 12535–12544.
Dehay, B., et al., 2013. Lysosomal impairment in Parkinson's disease. Mov. Disord. 28, 725–732.
Dlugosz, P., Nimpf, J., 2018. The Reelin receptors apolipoprotein E receptor 2 (ApoER2) and VLDL receptor. Int. J. Mol. Sci. 19, 3090.
Gao, J., et al., 2019. Autophagy activation promotes clearance of α-synuclein inclusions in fibril-seeded human neural cells. J. Biol. Chem. 294, 14241–14256.
Gelfo, F., et al., 2011. Enriched environment improves motor function and increases neurotrophins in hemicerebellar lesioned rats. Neurorehabil. Neural Repair 25, 243–252.
Giasson, B.I., et al., 2002. Neuronal α-synucleinopathy with severe movement disorder in mice expressing A53T human α-synuclein. Neuron. 34, 521–533.
Goldman, J.G., et al., 2018. Cognitive impairment in Parkinson's disease: a report from a multidisciplinary symposium on unmet needs and future directions to maintain cognitive health. npj Parkinson's Dis. 4, 1–11.
Graham, D.R., Sidhu, A., 2010. Mice expressing the A53T mutant form of human alpha-synuclein exhibit hyperactivity and reduced anxiety-like behavior. J. Neurosci. Res. 88, 1777–1783.
Hamm, R.J., et al., 1996. Exposure to environmental complexity promotes recovery of cognitive function after traumatic brain injury. J. Neurotrauma 13, 41–47.
Huang, J., et al., 2019. Exercise activates lysosomal function in the brain through AMPK-SIRT1-TFEB pathway. CNS Neurosci. Ther. 25, 796–807.
Janssen, H., et al., 2014. An enriched environment increases activity in stroke patients undergoing rehabilitation in a mixed rehabilitation unit: a pilot non-randomized controlled trial. Disabil. Rehabil. 36, 255–262.
Jesse, S., et al., 2009. Neurochemical approaches in the laboratory diagnosis of Parkinson and Parkinson dementia syndromes: a review. CNS Neurosci. Ther. 15, 157–182.
Kilpeläinen, T., et al., 2019. Behavioural and dopaminergic changes in double mutated human A30P*A53T alpha-synuclein transgenic mouse model of Parkinson's disease. Sci. Rep. 9, 17382.

Kim, J.E., et al., 2013. Treadmill exercise ameliorates motor disturbance through inhibition of apoptosis in the cerebellum of valproic acid-induced autistic rat pups. Mol. Med. Rep. 8, 327–334.
Kim, I., et al., 2017. Early-onset mild cognitive impairment in Parkinson's disease: altered corticopetal cholinergic network. Sci. Rep. 7, 1–10.
Kim, K., et al., 2021. Reduced interaction of aggregated α-synuclein and vamp2 by environmental enrichment alleviates hyperactivity and anxiety in a model of Parkinson's disease. Genes. 12, 392.
Kraeuter, A.K., et al., 2019. The Y-maze for assessment of spatial working and reference memory in mice. Methods Mol. Biol. 1916, 105–111.
Leger, M., et al., 2013. Object recognition test in mice. Nat. Protoc. 8, 2531–2537.
Lidón, L., et al., 2020. Disease-specific changes in Reelin protein and mRNA in neurodegenerative diseases. Cells. 9, 1252.
Livingston-Thomas, J., et al., 2016. Exercise and environmental enrichment as enablers of task-specific neuroplasticity and stroke recovery. Neurotherapeutics. 13, 395–402.
Lotharius, J., Brundin, P., 2002. Impaired dopamine storage resulting from alpha-synuclein mutations may contribute to the pathogenesis of Parkinson's disease. Hum. Mol. Genet. 11, 2395–2407.
Lueptow, L.M., 2017. Novel object recognition test for the investigation of learning and memory in mice. J. Vis. Exp. 126, e55718.
Magen, I., et al., 2012. Cognitive deficits in a mouse model of pre-manifest Parkinson's disease. Eur. J. Neurosci. 35, 870–882.
Majbour, N.K., et al., 2016. Oligomeric and phosphorylated alpha-synuclein as potential CSF biomarkers for Parkinson's disease. Mol. Neurodegener. 11, 1–15.
Malik, B.R., et al., 2019. Autophagic and endo-lysosomal dysfunction in neurodegenerative disease. Mol. Brain. 12, 100.
Marcon, M., et al., 2018. Environmental enrichment modulates the response to chronic stress in zebrafish. J. Exp. Biol. 221, jeb176735.
Martins, L.A., et al., 2022. The foot fault scoring system to assess skilled walking in rodents: a reliability study. Front. Behav. Neurosci. 16, 892010.
McGregor, M.M., Nelson, A.B., 2019. Circuit mechanisms of Parkinson's disease. Neuron. 101, 1042–1056.
Meadowcroft, M.D., et al., 2015. Cortical iron regulation and inflammatory response in Alzheimer's disease and APPSWE/PS1ΔE9 mice: a histological perspective. Front. Neurosci. 9, 255.
Metz, G.A., Whishaw, I.Q., 2002. Cortical and subcortical lesions impair skilled walking in the ladder rung walking test: a new task to evaluate fore-and hindlimb stepping, placing, and co-ordination. J. Neurosci. Methods 115, 169–179.
Middleton, F.A., Strick, P.L., 2000. Basal ganglia output and cognition: evidence from anatomical, behavioral, and clinical studies. Brain Cogn. 42, 183–200.
Moon, U.Y., et al., 2015. Impaired Reelin-Dab1 signaling contributes to neuronal migration deficits of tuberous sclerosis complex. Cell Rep. 12, 965–978.
Nam, J.H., et al., 2014. Induction of GDNF and BDNF by hRheb(S16H) transduction of SNpc neurons: neuroprotective mechanisms of hRheb(S16H) in a model of Parkinson's disease. Mol. Neurobiol. 51, 487–499.
Nam, J.H., et al., 2015. TRPV1 on astrocytes rescues nigral dopamine neurons in Parkinson's disease via CNTF. Brain. 138, 3610–3622.
Neureither, F., et al., 2017. Impaired motor coordination and learning in mice lacking anoctamin 2 calcium-gated chloride channels. Cerebellum. 16, 929–937.
Niethammer, M., et al., 2013. Parkinson's disease cognitive network correlates with caudate dopamine. Neuroimage. 78, 204–209.
Nithianantharajah, J., Hannan, A.J., 2006. Enriched environments, experience-dependent plasticity and disorders of the nervous system. Nat. Rev. Neurosci. 7, 697–709.
Niu, S., et al., 2008. The Reelin signaling pathway promotes dendritic spine development in hippocampal neurons. J. Neurosci. 28, 10339–10348.
Nygren, J., Wieloch, T., 2005. Enriched environment enhances recovery of motor function after focal ischemia in mice, and downregulates the transcription factor NGFI-A. J. Cereb. Blood Flow Metab. 25, 1625–1633.
Pang, T.Y., et al., 2019. Novel approaches to alcohol rehabilitation: modification of stress-responsive brain regions through environmental enrichment. Neuropharmacology. 145, 25–36.
Parnetti, L., et al., 2019. CSF and blood biomarkers for Parkinson's disease. Lancet Neurol. 18, 573–586.
Paumier, K.L., et al., 2013. Behavioral characterization of A53T mice reveals early and late stage deficits related to Parkinson's disease. PLoS One 8, e70274.
Peck, J.A., et al., 2015. Environmental enrichment induces early heroin abstinence in an animal conflict model. Pharmacol. Biochem. Behav. 138, 20–25.
Poewe, W., et al., 2017. Parkinson disease. Nat. Rev. Dis. Primers. 3, 17013.
Pujadas, L., et al., 2014. Reelin delays amyloid-beta fibril formation and rescues cognitive deficits in a model of Alzheimer's disease. Nat. Commun. 5, 3443.
Qin, H., et al., 2021. Environmental enrichment for stroke and other non-progressive brain injury. Cochrane Database Syst. Rev. 11, CD011879.
Qiu, S., et al., 2006. Differential reelin-induced enhancement of NMDA and AMPA receptor activity in the adult hippocampus. J. Neurosci. 26, 12943–12955.
Radabaugh, H.L., et al., 2017. Refining environmental enrichment to advance rehabilitation based research after experimental traumatic brain injury. Exp. Neurol. 294, 12–18.
Rassu, M., et al., 2017. Role of LRRK2 in the regulation of dopamine receptor trafficking. PLoS One 12, e0179082.
Rice, D.S., Curran, T., 2001. Role of the reelin signaling pathway in central nervous system development. Annu. Rev. Neurosci. 24, 1005–1039.
Rogers, J.T., et al., 2011. Reelin supplementation enhances cognitive ability, synaptic plasticity, and dendritic spine density. Learn. Mem. 18, 558–564.
Rosenzweig, M.R., et al., 1978. Social grouping cannot account for cerebral effects of enriched environments. Brain Res. 153, 563–576.
Sáez-Valero, J., et al., 2003. Altered levels of cerebrospinal fluid reelin in frontotemporal dementia and Alzheimer's disease. J. Neurosci. Res. 72, 132–136.
Sampedro-Piquero, P., Begega, A., 2017. Environmental enrichment as a positive behavioral intervention across the lifespan. Curr. Neuropharmacol. 15, 459–470.
Seo, T.-B., et al., 2013. Treadmill exercise improves behavioral outcomes and spatial learning memory through up-regulation of reelin signaling pathway in autistic rats. J. Exercise Rehabil. 9, 220.
Seo, J.H., et al., 2020. Environmental enrichment attenuates oxidative stress and alters detoxifying enzymes in an a53t α-synuclein transgenic mouse model of Parkinson's disease. Antioxidants. 9, 928.
Sharaf, A., et al., 2015. Localization of reelin signaling pathway components in murine midbrain and striatum. Cell Tissue Res. 359, 393–407.
Smith, B.R., et al., 2014. Neuronal inclusions of α-synuclein contribute to the pathogenesis of Krabbe disease. J. Pathol. 232, 509–521.
Tian, Y.H., et al., 2010. Prenatal and postnatal exposure to bisphenol a induces anxiolytic behaviors and cognitive deficits in mice. Synapse. 64, 432–439.
Tomlinson, C.L., et al., 2013. Physiotherapy versus placebo or no intervention in Parkinson's disease. Cochrane Database Syst. Rev. 2013, CD002817.
Tsukita, K., et al., 2021. Long-term effect of regular physical activity and exercise habits in patients with early Parkinson disease. Neurology. 98, e859–e871.
Turner, C.A., Lewis, M.H., 2003. Environmental enrichment: effects on stereotyped behavior and neurotrophin levels. Physiol. Behav. 80, 259–266.
Ułas, J., Cotman, C.W., 1996. Dopaminergic denervation of striatum results in elevated expression of NR2A subunit. Neuroreport. 7, 1789–1793.
Unger, E.L., et al., 2006. Locomotor hyperactivity and alterations in dopamine neurotransmission are associated with overexpression of A53T mutant human alpha-synuclein in mice. Neurobiol. Dis. 21, 431–443.
Venda, L.L., et al., 2010. α-Synuclein and dopamine at the crossroads of Parkinson's disease. Trends Neurosci. 33, 559–568.
Volpicelli-Daley, L.A., et al., 2011. Exogenous α-synuclein fibrils induce Lewy body pathology leading to synaptic dysfunction and neuron death. Neuron. 72, 57–71.
Wang, X.J., et al., 2020. Autonomic ganglionic injection of α-synuclein fibrils as a model of pure autonomic failure α-synucleinopathy. Nat. Commun. 11, 934.
Wassouf, Z., Schulze-Hentrich, J.M., 2019. Alpha-synuclein at the nexus of genes and environment: the impact of environmental enrichment and stress on brain health and disease. J. Neurochem. 150, 591–604.
Wenger, N., et al., 2022. Rodent models for gait network disorders in Parkinson's disease–a translational perspective. Exp. Neurol. 114011.
Wi, S., et al., 2018. An enriched environment ameliorates oxidative stress and olfactory dysfunction in Parkinson's disease with α-synucleinopathy. Cell Transplant. 27, 831–839.
Xilouri, M., et al., 2016. Autophagy and alpha-Synuclein: relevance to Parkinson's disease and related Synucleopathies. Mov. Disord. 31, 178–192.
Xu, C.L., et al., 2012. Asiaticoside: attenuation of neurotoxicity induced by MPTP in a rat model of Parkinsonism via maintaining redox balance and up-regulating the ratio of Bcl-2/Bax, 100. Pharmacol. Biochem. Behav., pp. 413–418
Xu, L., Pu, J., 2016. Alpha-Synuclein in Parkinson's disease: from pathogenetic dysfunction to potential clinical application. Parkinsons Dis. 2016, 1720621.
Yang, M., Crawley, J.N., 2009. Simple behavioral assessment of mouse olfaction. Curr. Protoc. Neurosci. 48, 8–24.
Yun, S.P., et al., 2018. Block of A1 astrocyte conversion by microglia is neuroprotective in models of Parkinson's disease. Nat. Med. 24, 931–938.